JSES International 7 (2023) 2445–2453

Contents lists available at ScienceDirect

JSES International

journal homepage: www.jsesinternational.org

Implications of humeral short-stem diametral sizing on implant stability

Jacob M. Reeves, PhD[a,b], Gregory W. Spangenberg, BESc[a,b], Josie A. Elwell, PhD[c], Ben Stewart, BSID[c], Tom Vanasse, MSE[c], Chris Roche, MSE, MBA[c], Kenneth J. Faber, MD, FRCSC[a,b], G. Daniel G. Langohr, PhD[a,b,*]

[a]*Department of Mechanical and Materials Engineering, The University of Western Ontario, London, ON, Canada*
[b]*The Roth | McFarlane Hand and Upper Limb Centre, London, ON, Canada*
[c]*Exactech, Inc., Gainesville, FL, USA*

ARTICLE INFO

Keywords:
Shoulder arthroplasty
Stem stability
Micromotion
Subsidence
Construct stiffness
Short stem
Oversizing

Level of evidence: Basic Science Study; Biomechanics

Background: Shoulder arthroplasty humeral stem design has evolved to include various shapes, coatings, lengths, sizes, and fixation methods. While necessary to accommodate patient anatomy characteristics, this creates a surgical paradox of choice. The relationship between the surgeon's selection of short-stem implant size and construct stiffness, resistance to subsidence and micromotion has not been assessed.

Methods: Eight paired cadaveric humeri were reconstructed with surgeon-selected (SS) and 2-mm diametrically larger (SS+2) short-stemmed press-fit implants. Each reconstruction was subjected to 2000 cycles of 90° forward flexion loading, and stem subsidence and micromotion were measured using optical tracking. Compressive stiffness of the stem-bone reconstruction was then assessed by applying a load in-line with the stem axis that resulted in 5 mm of stem subsidence.

Results: Increasing stem size by 2 mm resulted in the construct stiffness more than doubling compared to SS stems (−741 ± 243 N/mm vs. −334 ± 120 N/mm; $P = .003$; power = 0.971). These larger stems also subsided significantly less than their SS counterparts (SS: 1.2 ± 0.6 mm; SS+2: 0.5 ± 0.5 mm; $P = .029$; power = 0.66), though there were no significant changes in micromotion (SS: 169 ± 59 μm; SS+2: 187 ± 52 μm; $P = .506$; power = 0.094).

Conclusions: The results of this study highlight the importance of proper short-stem sizing, as a relatively small 2 mm increase in diametral size was observed to significantly impact construct stiffness, which could increase the risk of stress shielding and implant loosening. Future work should focus on developing tools that objectively quantify bone quality and aid surgeons in selecting the appropriate size short-stem humeral implants for a particular patient.

© 2023 The Authors. Published by Elsevier Inc. on behalf of American Shoulder and Elbow Surgeons. This is an open access article under the CC BY-NC-ND license (http://creativecommons.org/licenses/by-nc-nd/4.0/).

Anatomic shoulder arthroplasty humeral stem design has evolved to offer a variety of shapes, lengths, sizes and surface coatings. As these prostheses are more rigid than the bone they replace, shifting load transfer through the press-fit stem can unintentionally result in reduced loading of the proximal cortex, a phenomena known as stress shielding.[14,37] Stress shielding can lead to bone resorption, like that noted in 69% of the stems used by McElwain in his 1984 investigation of a porous-coated standard-length stem design.[23] Similarly, Nagel et al[25] found cortex thinning in 9% of their standard press-fit stems, which was significantly associated with stem thickness (fill ratio = 0.57 vs. 0.48; $P = .013$); though they posited that the true resorption incidence was higher because they were unable to assess cancellous changes.

To minimize the occurrence of stress shielding, humeral components have since evolved to short-stemmed and stemless metaphyseal designs to preserve bone stock and improve load distribution between the implant and bone. A direct comparison using finite element methods by Razfar et al[29] demonstrated that reducing stem length creates proximal stress distributions that better match those of the intact humerus. This is supported by in vivo work by Denard et al,[9] who showed a reduction in the prevalence of medial cortical thinning from 74% to 50% when short-stemmed humeral components were used instead of standard-length stems. Despite these improvements, concerns regarding stress shielding[2,32] and radiolucent lines[15] following short-stem

Ethical committee approval was not required for this cadaveric investigation.

*Corresponding author: G. Daniel G. Langohr, PhD, Lawson Health Research Institute, 268 Grosvenor Street, London, Ontario N6A 4L6, Canada.
E-mail address: glangohr@uwo.ca (G.D.G. Langohr).

https://doi.org/10.1016/j.jseint.2023.06.023
2666-6383/© 2023 The Authors. Published by Elsevier Inc. on behalf of American Shoulder and Elbow Surgeons. This is an open access article under the CC BY-NC-ND license (http://creativecommons.org/licenses/by-nc-nd/4.0/).

humeral arthroplasty persist. For example, Casagrande et al[7] reported a revision rate of 8.2% attributed to implant loosening in a series of 73 short, press-fit humeral components for total shoulder arthroplasty (TSA), and Aibinder et al[2] reported medial calcar resorption in 20% of 35 total shoulder arthroplasty and 24% of 65 reverse shoulder arthroplasty short stems.

Recent assessments have focused on whether there are benefits or tradeoffs associated with the diametral sizing (ie, thickness) of short-stemmed humeral components.[18,27,28,32,33] To assess this, studies report the metaphyseal fill ratio (FR_{met}) and diaphyseal fill ratio (FR_{dia}) as the division of stem thickness over bone thickness at 2 predefined locations on an anteroposterior radiograph.[32] Though these terms are commonly used to describe the fill ratios of standard length and short-stemmed humeral implants, as seen in Fig. 1, they may be more accurately described as proximal and distal FRs when discussing short stems because these implants do not traverse as deeply into the diaphysis. The findings of these investigations support the belief that larger, stiffer stems may cause greater stress shielding.[13,37] In fact, significantly higher rates of bone adaptations have been reported by Schnetzke et al[32] ($P \leq .007$) and Raiss et al[28] ($P \leq .003$) in uncemented short-stem reconstructions with high fill ratios. Specifically, Raiss et al[28] found that the relative risk for high bone adaptations was 4 times greater if the stem produced a $FR_{dia} \geq 0.7$ ($P = .006$).

When selecting the appropriate size of short-stem implant, surgeons are given little objective guidance, leading them to rely on tactile assessments of stem stability.[28,32] Immediate stability is typically evaluated via tactile assessment of rotation and pistoning, while ultimately the assessment is done via either radiographic subsidence or experimental stem micromotion testing. To date, there have not been any studies investigating the micromotion of short stem humeral arthroplasty. Accordingly, in the pursuit of quantifying metrics to aid in selecting the most appropriate short stem implant for shoulder arthroplasty patients, it is important to understand how a stem's diametral (ie, thickness) sizing impacts stability; this study investigates this relationship. It is hypothesized that oversizing a short-stem component would result in significantly larger FRs, as well as a stiffer overall construct, which may result in a greater resistance to subsidence and less micromotion.

Methods

Subject demographics and preparation

Eight paired male cadaveric shoulders (age = 74.8 ± 15.2 years; weight = 66 ± 10 kg [146 ± 23 lbs]) were procured and screened for bone defects via an intake computed tomography (CT) scan. The proximal humerus was then resected at the mid-diaphysis and denuded of all soft tissues. An orthopedic surgeon (K.J.F.) with more than 20 years of experience resected the humeral head and all specimens were CT scanned to capture the resection orientation. Each scan was performed with a density phantom (qCT Pro model 3; Mindways Software, Austin, TX, USA) within the field-of-view, to permit the calibration of CT attenuation (Houndsfield units) to K_2HPO_4 (dipotassium phosphate) equivalent density (g/cm^3).[17]

Each proximal humerus was then segmented from its surrounding using 3D Slicer[16] (version 4.11.2; https://www.slicer.org/) and 3D models were constructed of the cortex and metaphyseal cancellous regions. Morphological assessments have indicated that bone density significantly diminishes 20 mm distal to the humeral head resection plane.[30] Accordingly, the metaphyseal region corresponding to the first 20 mm beneath the resection was isolated, and its density and volume were quantified (Table I).

Each humeral pair was then randomized into 2 groups to test the effect of stem diametral sizing (ie, thickness). All humeri were reconstructed with the Preserve short-stem humeral implant (Exactech, Inc., Gainesville, FL, USA) using the manufacturer's surgical technique guide. The humeral head was resected with an extramedullary 132.5° guide and the canal was sequentially broached until the surgeon determined through subjective tactile assessment that satisfactory rotational broach stability had been achieved. A 2 mm offset collar used during broaching intentionally left the definitive implant stem seated slightly proud of the resection plane. This allowed initial stem stability to be assessed prior to achieving head-back contact. The first humerus was implanted with the surgeon-selected (SS) stem, which was sized based on the surgeon's tactile assessment of the smallest broach that provided stem resistance to torsional loading. Then, the contralateral limb was reconstructed using a stem that was 2 mm (SS+2) larger diametrically. Per the stem design, all reconstructions resulted in fits that relied on compacted cancellous tissue for support, such that no stem completely filled the humeral canal. Following reconstruction, each specimen was radiographed and the stem FRs were measured according to the method presented by Raiss et al and Schnetzke et al[28,32,33] (Fig. 1). The resulting FR_{met} and FR_{dia} were 0.50 ± 0.10 and 0.45 ± 0.07 for the SS stems and 0.50 ± 0.06 and 0.52 ± 0.06 for the SS+2 stems, respectively (Table I).

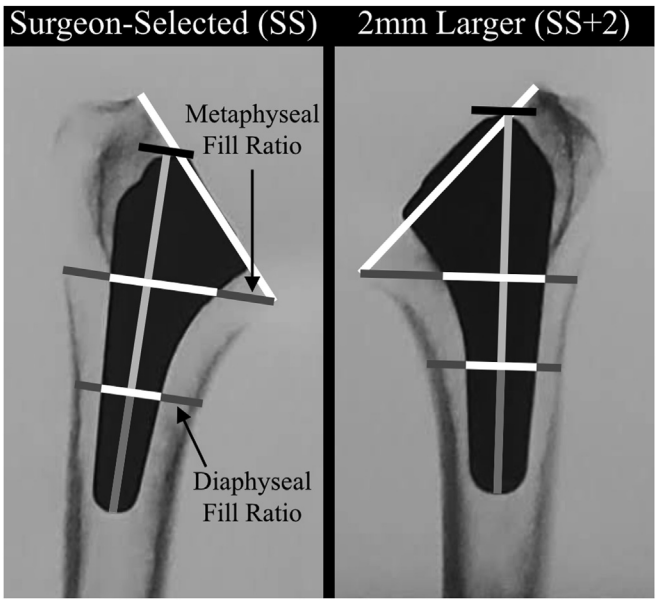

Figure 1 Antero-posterior radiographs of one pair of implanted short humeral stems. Lines indicated the assessment lengths used to quantify metaphyseal and diaphyseal fill-ratios. *SS,* surgeon-selected.

A custom loading adapter intentionally positioned the humeral head 2 mm above the resection surface and was affixed to the stem to permit direct load application and the rigid attachment of an optical tracker (Optotrak Certus; Northern Digital Inc., Waterloo, ON, Canada) (Fig. 2, *A*). This system was constructed to mimic complete coverage of the resection surface by a humeral head that was locked into position with a fixed neck-shaft angle of 132.5° once the loading adapter was centralized on the resection surface. This differs from the implant design, which additionally permits some variability in head-neck angle to further accommodate patient geometry. Each humerus was cut 14 cm distal to the greater tuberosity and potted in a 7.6 cm tube using PMMA (polymethyl methacrylate) bone cement, which was filled to 5 mm beneath the humeral head resection (Fig. 2). A second optical tracker was rigidly affixed to the humeral pot to permit tracking the relative movement of the stem with respect to the proximal humerus. Previous

Table I
Specimen and reconstruction statistics for surgeon-selected and 2 mm larger stem pairings.

	Stem condition	Specimen pair								Mean (SD)	*P* value (power)
		1	2	3	4	5	6	7	8		
Metaphyseal region-of-interest (ROI)											
K_2HPO_4 equivalent density [g/cm^3]	Surgeon-Selected	32.5	52.1	31.3	4.3	92.5	45.3	70.2	20.5	43.6 (28.1)	.279
	2 mm Larger	37.8	67.7	44.9	3.2	75.9	55.7	72.9	24.3	47.8 (25.4)	(0.175)
RoI volume [cm^3]	Surgeon-Selected	21.9	19.7	22.8	22.9	19.8	19.9	22.1	28.7	22.2 (2.9)	.852
	2 mm Larger	20.7	20.6	22.5	23.7	20	19.3	23.5	28	22.3 (2.8)	(0.053)
Reconstruction metrics											
Stem size	Surgeon-Selected	9	9	12	9	6	8	8	10	9 (2)	N/A
	2 mm Larger	11	11	14	11	8	10	10	12	11 (2)	N/A
Metaphyseal fill ratio (0-1.0)	Surgeon-Selected	0.51	0.54	0.60	0.56	0.34	0.53	0.58	0.37	0.50 (0.10)	.997
	2 mm Larger	0.47	0.49	0.54	0.56	0.40	0.57	0.56	0.44	0.50 (0.06)	(0.050)
Diaphyseal fill ratio (0-1.0)	Surgeon-Selected	0.47	0.52	0.55	0.47	0.34	0.47	0.42	0.40	0.45 (0.07)	<.001
	2 mm Larger	0.52	0.54	0.62	0.53	0.42	0.54	0.49	0.48	0.52 (0.06)	(1.000)
Construct stiffness (N/mm)	Surgeon-Selected	−307	−292	−166	−290	−519	−409	−228	−463	−334 (120)	.003
	2 mm Larger	−790	−925	−775	−279	−992	−925	−755	−485	−741 (243)	(0.971)

work has indicated that using this optical tracking system with rigid body referencing has a precision of 9.7-14.9 μm, a repeatability of 0.9-10.0 μm, and within- and out-of-plane accuracies less than 15 μm for displacements ≤1 mm, provided that the rigid bodies remain static during each successive position capture (manuscript under review). The specimen was then secured in a rigid arc fixed to an XY-stage that allowed the specimen's anatomic adapter to be positioned directly beneath the actuator of an Instron 8501 materials testing machine (Instron Inc., Norwood, MA, USA).

Anatomic stability assessment

To mimic a clinically relevant postoperative loading scenario, in vivo telemetrized humeral implant data from 6 tests with 3 patients were obtained from the OrthoLoad database (orthoload.com).[3,4,12,36] This data indicated that the mean humeral load corresponding to 90° of forward elevation is 75% bodyweight (BW), oriented at 18.5° of retroversion and 47.5° from the diaphyseal axis. Since humeral head retroversion has been quantified as 17.9° ± 13.4°[6] and the Preserve stem's head-neck angle is 42.5°, articular loading was oriented perpendicular to the humeral head resection plane, passing through the center of curvature of the anatomic loading adapter (Fig. 2, *A*).

The Instron machine was placed in load control and each stem was subjected to a static 10 N preload[8] while the initial orientation of the stem was captured relative to the humerus for a duration of 10 seconds. This was repeated with a load of 75% BW, then again with another static 10 N load to assess the stem's movements in response to the initial load application. Following this, the stem was cyclically loaded between 10 N and 75% BW (specimen specific range: 400-608 N) at a rate of 1 Hz[8] for a total of 2000 cycles. To assess stem displacement over time, the cyclic loading was paused after 10, 25, 50, 100, 200, 400, 600, 800, 1000, 1500, and 2000 cycles at which time the stem orientation was again captured under a static preload of 10 N, then a static anatomic load of 75% BW. Using these stem orientations and a stem coordinate system formed from points digitized prior to testing, subsidence and micromotion were calculated at 4 points: the center of the medial and lateral edges of the stem's proximal surface, the stem's center-of-mass (CoM), and the distal stem tip (Fig. 3).

Subsidence was calculated as the resultant change in position of these points when subjected to the static preload of 10 N between each cyclic intervals.[5,20,22,24] Additionally, the cumulative subsidence was calculated by comparing the initial stem position to that of the final position after 2000 cycles of loading. Micromotion was then calculated by comparing each point's displacement from the preloaded to anatomically loaded positions following each cyclic loading interval.[1,8,11] Finally, the rotation of the stem was quantified about the stem axis, as well as the anterior-posterior and medial-lateral axes, both for subsidence and micromotion. Visual depictions of the subsidence and micromotion definitions with respect to the loading sequence are shown in Fig. 2, *A*.

Construct stiffness testing

Following the anatomic loading assessment, the stem's anatomic adapter was replaced with a stem axis loading adapter (Fig. 2, *B*). This adapter was designed without a collar to isolate the effect of stem size on the stem's resistance to forced subsidence, independent of the implant's head-back contact. The humerus was oriented such that the stem axis was vertical and in-line with the applied force and the Instron machine was placed in displacement control. The loading actuator was manually moved until it began contacting the stem's loading adapter, then the stem was forcefully displaced into the humerus to a maximum subsidence of 5 mm[31] to equal the mean humeral stem subsidence reported by Sanchez-Sotelo et al.[10,21,35] This forced subsidence occurred at a rate of 1 mm/minute, matching previous assessments of cancellous material properties and acetabular implant push-out. Force and displacement data were collected at a rate of 100 Hz. The stem's resistance to forced subsidence was quantified by its compressive construct stiffness (N/mm), which was measured as the slope of the linear section of the resulting force-displacement curve.[19]

The effect of stem size on subsidence, micromotion, and construct stiffness was assessed using paired *t* tests; with alpha set at .05. The correlation between each outcome variable and the FRs was also assessed.

Results

The most commonly used SS-sized stem was 9 mm, though stems chosen ranged from 6 to 12 mm (6 mm: 1, 8 mm: 2, 9 mm: 3, 10 mm: 1, and 12 mm: 1). The corresponding SS+2 stems were 2 mm larger than their paired counterparts, resulting in a range of 8-14 mm, with the most common being an 11-mm stem (8 mm: 1, 10 mm: 2, 11 mm: 3, 12 mm: 1, and 14 mm: 1). No significant differences were found between the SS and SS+2 groups in terms of the metaphyseal region-of-interest's volume ($P = .852$; power = 0.053),

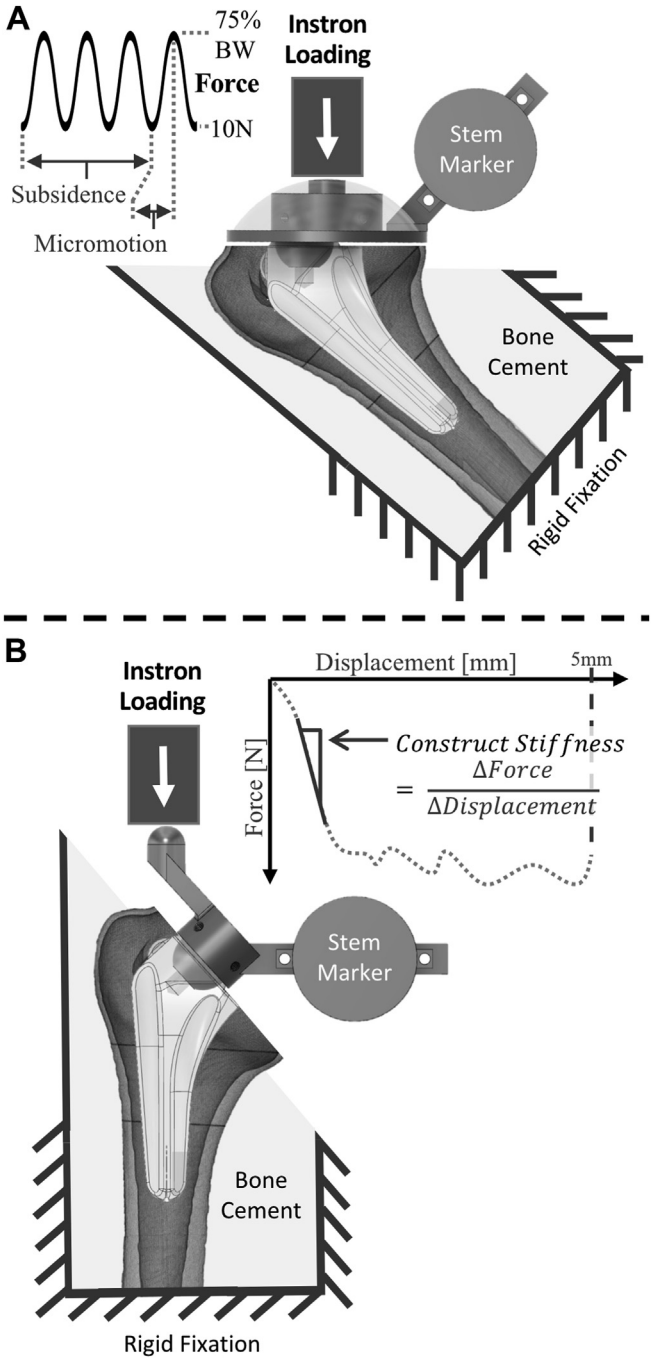

Figure 2 Custom stem adapters were developed to rigidly attach an optical tracking marker to the stem, while also allowing for anatomic (**A**) and construct stiffness (**B**) loading, corresponding to 90° of forward flexion and coincident to the stem axis, respectively.

its K_2HPO_4-equivalent density ($P = .279$; power = 0.175), or the FR_{met} ($P = .997$; power = 0.050; Table I); however, the diaphyseal FR was significantly larger for the SS+2 stems (0.52 ± 0.06 vs. 0.45 ± 0.07; $P < .001$; power = 1.000).

FRs (metaphysis: $P \geq .067$; diaphysis: $P \geq .296$), micromotion (metaphysis: $P \geq .600$; diaphysis: $P \geq .188$), or construct stiffness (metaphysis: $P = .259$; diaphysis: $P = .529$) were not significantly correlated with stem subsidence.

Subsidence

Subsidence resulted in head-back contact in 75% (6 of 8) of the SS-sized stems, but only 12.5% (1 of 8) of the SS+2 stems. SS stem head-back contact remained elusive in the two highest density specimens (92.5g/cm^3 and 70.2g/cm^3), while it only occurred for the SS+2 stem in the lowest density specimen (3.2g/cm^3). Regardless of stem size, subsidence was primarily perpendicular to the humeral head resection, in-line with the applied force, resulting in the stem moving inferiorly and laterally (Table II). At the lateral point, the SS+2 stem's subsidence was significantly less than the SS stem only following the initial load application ($P = .024$; power = 0.653); following this, the subsidence was not significantly different between stem sizes for subsequent intervals ($.144 \leq P \leq .951$, $.050 \leq$ power ≤ 0.296; Fig. 3). Stem subsidence was also less for the SS+2 stems compared to the SS stems for the other points-of-interest (Fig. 3); however, the significance shifted after the first 10 cycles of loading for the stem's medial point ($P = .023$, power = 0.698), CoM ($P = .015$, power = 0.786), and stem tip ($P = .037$, power = 0.598), with subsidence otherwise not being significantly different for the initial load application or at any of the other cyclic intervals (ie, 25-2000 cycles) (medial: $.070 \leq P \leq .880$; $0.052 \leq$ power ≤ 0.454; CoM: $.055 \leq P \leq .917$; $0.051 \leq$ power ≤ 0.509; stem tip: $.054 \leq P \leq .901$; $0.051 \leq$ power ≤ 0.515). The mean stem rotations did not exceed 1° about any axis and were not significantly different after 2000 cycles of loading (x: $P = .168$, power = 0.266; y: $P = .325$, power = 0.151; and z: $P = .274$, power = 0.178).

Subsidence plateaued for all points after approximately 400 cycles of humeral loading, regardless of stem size, after which the percentage increase ranged from 0% to 2% for SS stems and 2%-4% for SS+2 stems at each subsequent interval. A visual comparison of the average subsidence of the SS and SS+2 stems after 2000 cycles of anatomic loading is presented in Fig. 4. Following 2000 cycles of loading, the cumulative SS stem subsidence was 1.17 ± 0.7 mm at the lateral point, 1.3 ± 0.7 mm at the medial point, 1.2 ± 0.6 mm at the stem's CoM, and 1.8 ± 1.0 mm at the stem tip, whereas the SS+2 stems subsided by 0.6 ± 0.6 mm at the lateral point, 0.5 ± 0.5 mm at the medial point, 0.5 ± 0.5 mm at the stem's CoM and 0.7 ± 0.7 mm at the stem tip (Fig. 3). These cumulative differences were significant for the medial point ($P = .040$; power = 0.580), CoM ($P = .029$; power = 0.656), and stem tip ($P = .040$; power = 0.583), but not the lateral point ($P = .074$; power = 0.441).

Micromotion

Similarly, stem micromotion was also predominantly perpendicular to the humeral head resection plane (Table II). The mean micromotion of SS-sized stems was larger than that of SS+2 stems during the initial load application; however, this trend reversed following, at most, 400 cycles of loading (Fig. 5). No significant differences were found between the resultant micromotion of SS and SS+2 stems at any time point throughout the 2000 cycles of loading, nor were there any significant differences in stem rotations between stem sizes ($.096 \leq P \leq .896$; $.052 \leq$ power ≤ 0.383), with rotations about all axes again remaining less than 1°.

Micromotion plateaued following 400 cycles of loading, after which point the change between intervals ranged from 0% to 5% for SS stems, and 0%-3% for SS+2 stems. Again, a visual comparison between SS and SS+2 stem micromotion following 2000 cycles of loading is presented in Fig. 6. At this point, the resultant micromotion of the SS stem was 180 ± 53 μm at the lateral point, 165 ± 62 μm at the medial point, 169 ± 59 μm at the stem CoM, and 191 ± 95 μm at the stem tip; whereas the SS+2 stem's micromotion was

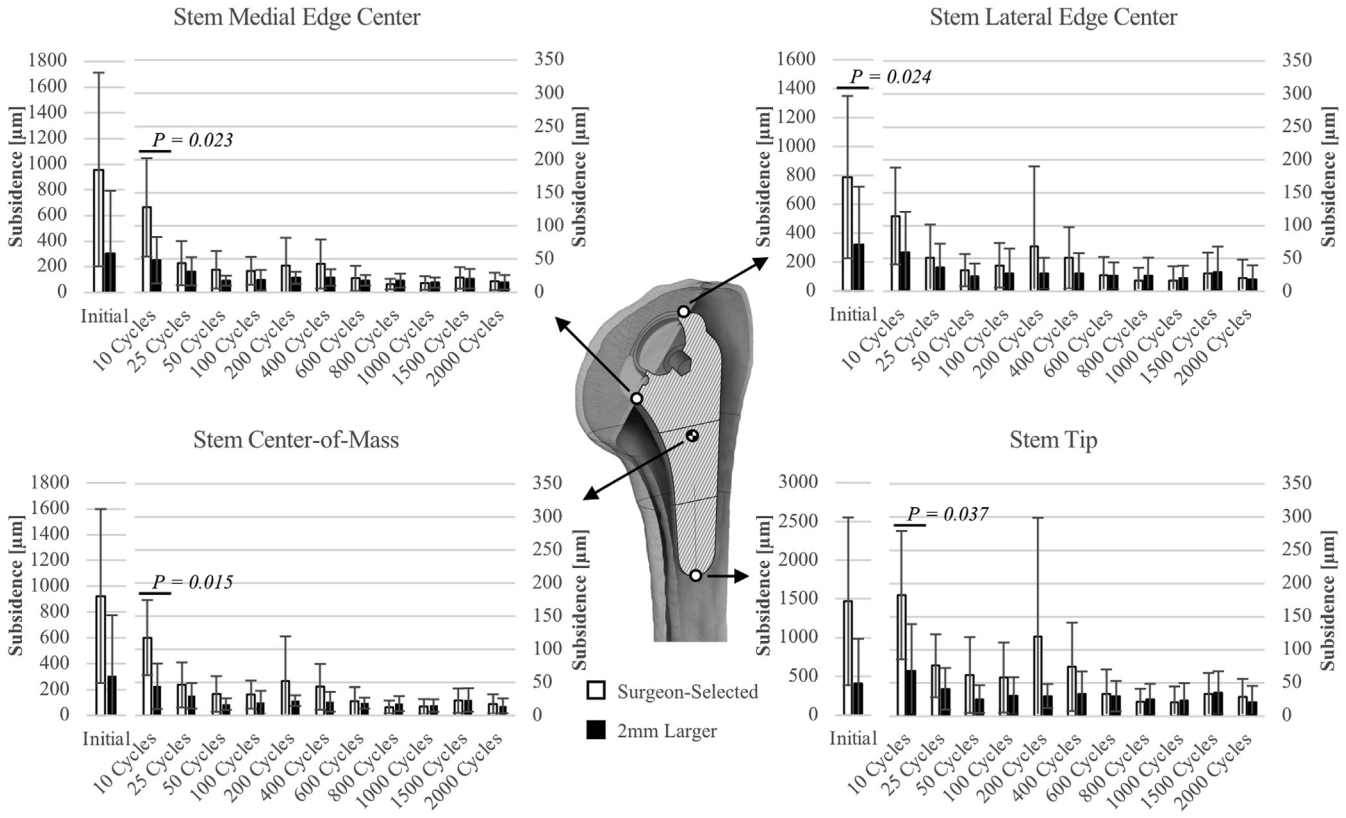

Figure 3 Mean ± standard deviation (shown as gray bars) graphs of the resultant incremental stem subsidence (µm) at 12 time points during anatomic cyclic loading.

191 ± 76 µm at the lateral point, 190 ± 51 µm at the medial point, 187 ± 52 µm at the stem CoM, and 207 ± 108 µm at the stem tip (Fig. 5).

Construct stiffness

Increasing the stem size by 2 mm had a significant impact on the stiffness of the stem-bone construct ($P = .003$, power = 0.971; Fig. 7). Increasing stem size by 2 mm yielded a construct stiffness of −741 ± 243 N/mm, more than double that of the standard stems, which was −334 ± 120 N/mm (Table I).

Discussion

The present results suggest that increasing short-stemmed humeral component size by 2 mm results in the creation of a stiffer bone-implant construct that resists subsidence more than its SS-sized counterparts during initial loading; however, no significant differences in stem micromotion were observed regardless of stem size. The diaphyseal FR and construct stiffness were significantly larger when an SS+2 short-stem prosthesis was used. Similarly, the SS+2 construct demonstrated less subsidence than the paired SS sized stems; however, the FR_{met} was not significantly different between the 2 groups. This is at least in part because the FR at the diaphysis is more sensitive to changes in stem diametral (ie, thickness) sizing, and is attributed to the smaller stem and bone cross-sections at the diaphyseal level, which causes a 2 mm increase in stem thickness to have a larger impact on the FR.

SS+2 short stems had a construct stiffness that was more than double that of the SS stems, though the micromotion was not significantly different between the 2 stem sizes. In a previous investigation, Lill et al[19] observed that high initial implant construct stiffness leads to early loosening and failure of the bone-implant interface. This suggests that even a small increase in stem sizing may have implications for short stem stability. These results may, in part, be attributed to the overly compacted adjacent cancellous bed that is formed from additional broaching, though this must be assessed in a future study.

The mean FR_{met} and FR_{dia} of the SS (0.50 ± 0.10 and 0.45 ± 0.07) and SS+2 (0.50 ± 0.06 and 0.52 ± 0.06) stems from the present investigation match well with the smaller (0.48 ± 0.03 and 0.44 ± 0.02) and larger (0.54 ± 0.04 and 0.50 ± 0.02) implants used in Langohr et al's[18] finite element investigation, which also utilized the Preserve short stem implant. Per their conclusion, the small reduction in diaphyseal FR seen between larger and SS stems may also reduce the risk of humeral stress shielding. This is supported by the significantly higher construct stiffness found with larger stems, and the decreased bone stimulus associated with the introduction of stiffer implants.[14]

Stem subsidence was generally most pronounced during the first 25 cycles of loading, while micromotion was found to decrease as the stem settled into place with additional cycles. Both subsidence and micromotion plateaued after 400 cycles at all 4 of the stem surface points assessed. This is considerably longer than the 25-100 cycles reported by Favre et al[11] for the micromotion of their stemless implants to stabilize; however, our setup intentionally positioned the backside of the loading adapter (which simulated the humeral head) 2 mm above the resection surface so that we could isolate the impact of stem size on stability independent of head-back contact. Stem subsidence did eventually lead to head-back contact in 75% of the SS stems studied, but only 12.5% of the SS+2 stems. This is an interesting finding, as head-back contact is an important mechanism for implant-bone load transfer that is thought to reduce stress-shielding induced bone resorption in the

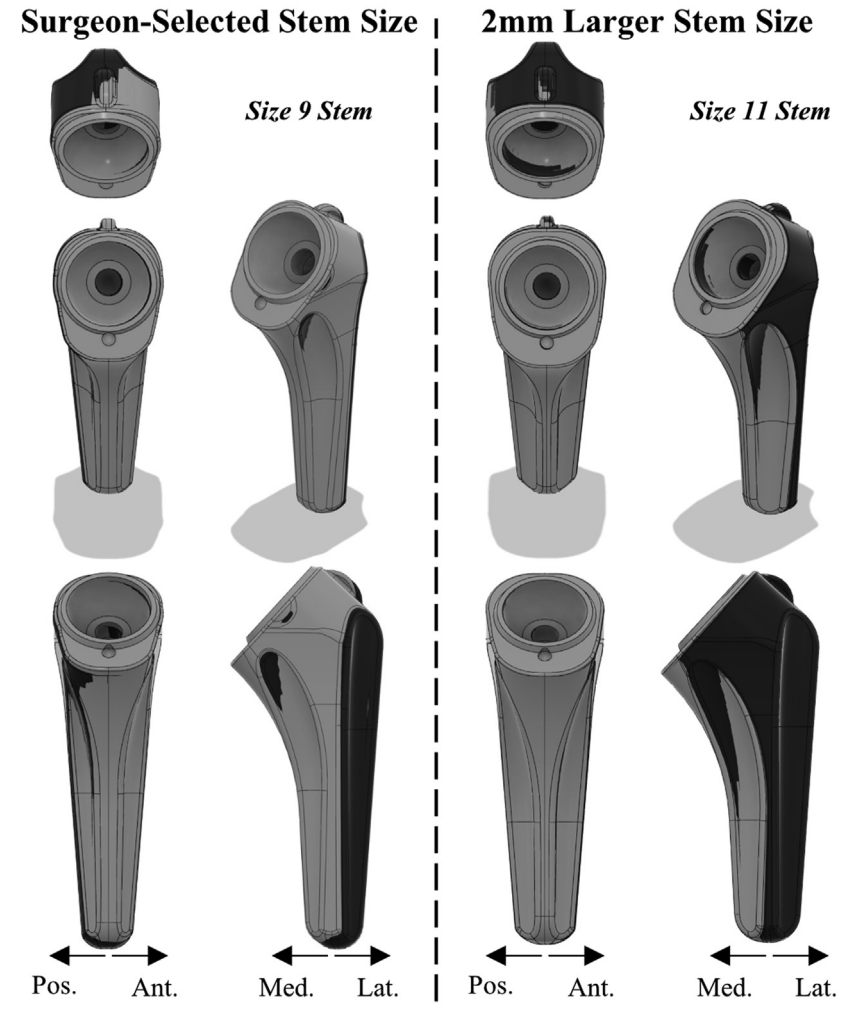

	Surgeon-Selected			2mm Larger		
	+Anterior - Posterior	*+Lateral -Medial*	*+Superior -Inferior*	*+Anterior - Posterior*	*+Lateral -Medial*	*+Superior -Inferior*
CoM Translation [μm]	-225 (681)	919 (548)	-785 (432)	86 (230)	388 (409)	-247 (352)
Rotation [°]	0.2(1.4)	0.2(0.7)	0.2(1.1)	0.4 (0.8)	0.0 (0.2)	0.0 (0.4)

Subsidence @ 2000 Cycles

Figure 4 Visualization of the mean (standard deviation) stem subsidence following 2000 cycles of anatomic loading. The light grey stem depicts the initial stem position, with the darker stem representing its final position. *CoM*, center of mass; *Med*, medial; *Lat*, lateral; *Ant*, anterior; *Pos*, posterior.

proximal humerus.[34] Accordingly, it is advised that surgeons avoid leaving a head-back gap as this will inhibit initial subsidence and encourage proximal load transfer.

Our testing configuration directly loaded the humeral stem to isolate differences in motion between 2 different short humeral stem sizes in matched pair cadaveric humeri. This testing configuration resulted in micromotion of both stem sizes that exceeded, but approached, the 150 μm threshold suggested by Pilliar et al[26] as the limit at which bone ingrowth is more likely to occur. Substantially less motion would be expected clinically if the humeral head were directly positioned on the resected bone, distributing the load throughout the proximal humerus as opposed to isolating the full load directly to the humeral stem. Surgeons are encouraged to impact the humeral head flush with the resected surface. Additionally, despite the displacement accuracy of the optical tracking system being less than 15 μm in and out of plane, it cannot account for deflection of the cancellous tissue directly surrounding the implant. As a result, the micromotion between the cancellous tissue and the implant may be less than is currently reported, as deflection of the cancellous structure in contact with bone may be contributing to the measured micromotion. Since this was consistent for both SS and SS+2 stems, this approach is appropriate for

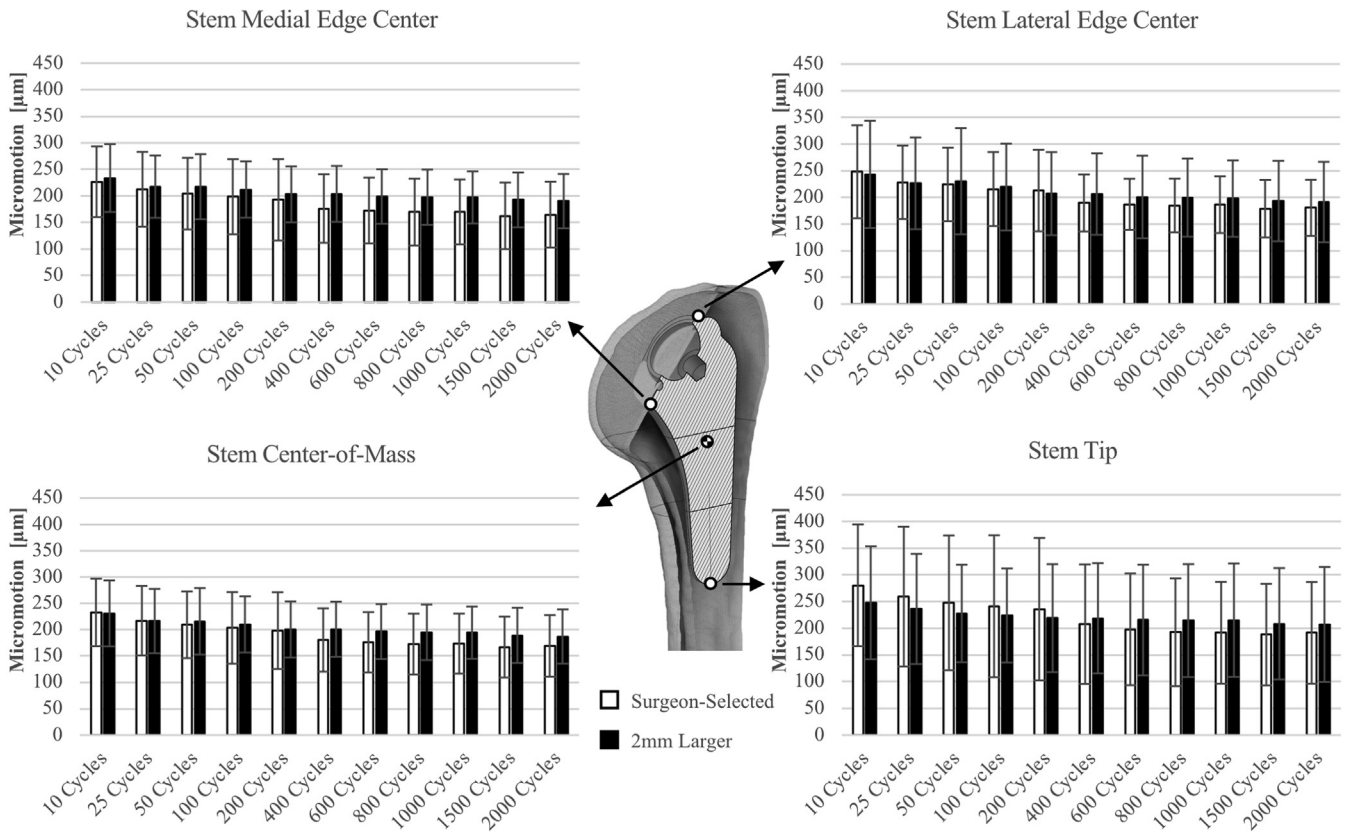

Figure 5 Mean ± standard deviation graphs of the resultant micromotion (μm) of the stem at each of the 12 time points during anatomic cyclic loading.

Table II
Breakdown of the mean stem subsidence and micromotion following 2000 cycles of loading according to the percentage contribution of the inferior, medial and anterior/posterior movements.

Location	Stem condition	Subsidence			Micromotion		
		Inf/sup	Med/lat	Ant/post	Inf/sup	Med/lat	Ant/post
		+Superior	+Lateral	+Anterior	+Superior	+Lateral	+Anterior
		−Inferior (%)	−Medial (%)	−Posterior (%)	−Inferior (%)	−Medial (%)	−Posterior (%)
Stem tip	Surgeon selected	−36	53	−11	−50	47	3
	2 mm larger	−42	44	14	−31	59	10
Stem CoM	Surgeon selected	−41	48	−12	−45	53	2
	2 mm larger	−34	54	12	−33	63	3
Medial point	Surgeon selected	−43	45	−11	−42	57	−1
	2 mm larger	−28	59	12	−32	62	−6
Lateral point	Surgeon selected	−43	44	−12	−43	56	1
	2 mm larger	−31	58	11	−34	65	0

Inf, inferior; *Sup*, superior; *Med*, medial; *Lat*, lateral; *Ant*, anterior; *Post*, posterior; *CoM*, center-of-mass.
To find what percentage of the resultant motion occurs in each direction

comparative analyses of implant displacements. It is also worth noting that the 150 μm reported by Pillar et al[11] was an assessment of uniaxial displacement, not 3D motion, and has been regarded as imprecise.

A related limitation of the present investigation is the use of a cadaveric model, with a limited number of 8 paired humeri. Though cadaveric testing does allow the humeral stems to be assessed in a controlled manner within the inhomogeneous and anisotropic cancellous bed of the proximal humerus, it cannot recreate the bone ingrowth provided by living tissue. Therefore, cyclic loading was ceased after 2000 cycles, at which time construct stiffness testing began. Two thousand cycles was chosen as the cyclic loading limit in order to double the 1000 cycles assessed in prior acetabular work by Crosnier et al,[8] and this far exceeds the 300 cycles reported by Favre et al.[11] Since implant subsidence and micromotion stabilized after 400 cycles, it is unlikely that further loading would have yielded additional clinically relevant findings in a cadaveric model incapable of simulating bone ingrowth. Future investigations should seek to replicate these findings in larger cadaveric populations to improve study power and better account for geometric and sex diversity.

The observed stem movements were generally perpendicular to the resection plane, approximately in-line with the orientation of the cyclic anatomic loading. It is possible that selecting the load orientation to match alternative activities of daily living may result in the stem subsidence and micromotion being oriented

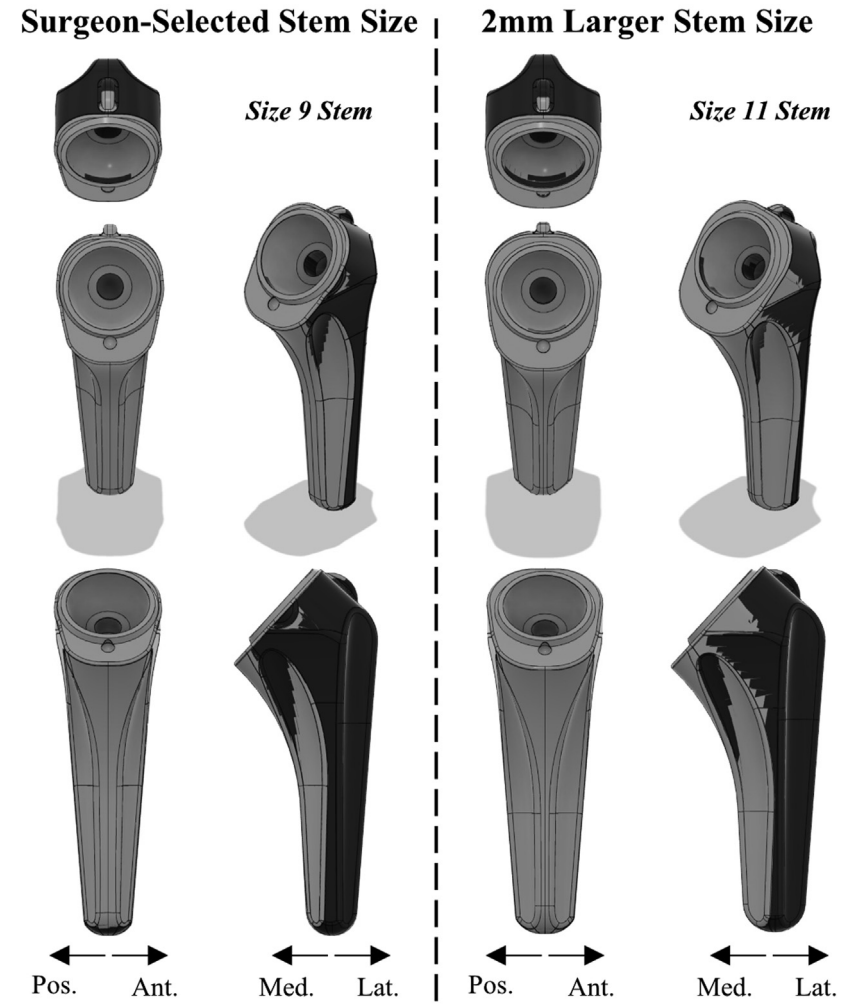

	Surgeon-Selected			2mm Larger		
	+Anterior - Posterior	*+Lateral -Medial*	*+Superior -Inferior*	*+Anterior - Posterior*	*+Lateral -Medial*	*+Superior -Inferior*
CoM Translation [μm]	4 (31)	125 (60)	-106 (27)	9 (27)	162 (49)	-85 (29)
Rotation [°]	0.0 (0.1)	0.0 (0.1)	0.0 (0.1)	0.0 (0.2)	0.0 (0.1)	-0.1 (0.1)

Micromotion @ 2000 Cycles

Figure 6 Visualization of the mean (standard deviation) stem micromotion following 2000 cycles of anatomic loading. The light grey stem depicts the initial stem position, with the darker stem representing its final position. *CoM*, center of mass; *Med*, medial; *Lat*, lateral; *Ant*, anterior; *Pos*, posterior.

differently; though Bergmann et al's[3] in vitro telemetrized implant data suggest that the orientation of glenohumeral loads remains fairly consistent.

Conclusions

Based on the results of this study, it appears that increasing the diametral size of short-stem humeral implants for anatomic shoulder arthroplasty produces significantly stiffer implant-bone constructs, which resist initial implant subsidence without causing a significant change in micromotion. A relatively small increase of 2 mm in short-stem sizing dramatically increased construct stiffness. This construct stiffness difference may have consequences on long-term clinical stress shielding and early loosening of the implant-bone interface.[19] To mitigate this risk along with the subjective nature of existing techniques for intra-operative stem sizing, which primarily rely on tactile assessments of broach fit,[28,32] future work should focus on the development of tools which objectively assesses an individual patient's bone quality. Such tools would aid surgeons in the selection of an ideal short-stem size for a given patient; by improving implant stability and mitigating stress shielding and premature stem failure.

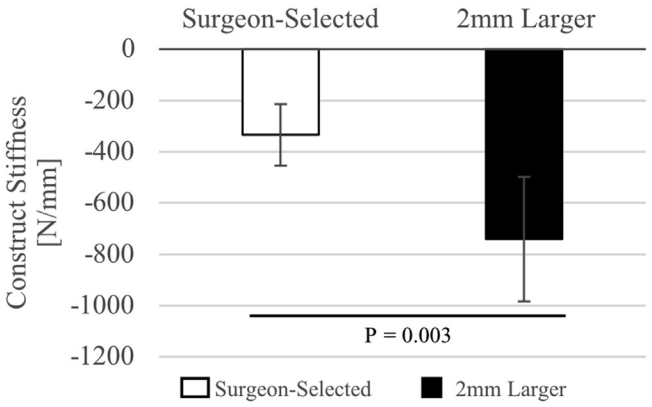

Figure 7 Mean ± standard deviation construct stiffness (N/mm) of the SS and SS+2 stems after 2000 cycles of anatomic loading. *SS*, surgeon-selected.

Disclaimers:

Funding: Funding for this work was provided by NSERC: 05346-2019 RGPIN and Mitacs: IT18239 ON-ISED.

Conflicts of interest: Jacob M. Reeves was a Mitacs Postdoctoral fellow during this investigation and his operating grant was funded in part by Exactech. Josie A. Elwell, Ben Stewart, Tom Vanasse, and Chris Roche are employees of Exactech Inc. Kenneth J. Faber is a consultant for Exactech Inc and receives royalties for implant development related to the subject of this article. The other authors, their immediate families, and any research foundation with which they are affiliated have not received any financial payments or other benefits from any commercial entity related to the subject of this article. Exactech Inc. had no input into this research project in any manner.

References

1. Abdic S, Lockhart J, Alnusif N, Johnson JA, Athwal GS. Glenoid baseplate screw fixation in reverse shoulder arthroplasty: does locking screw position and orientation matter? J Shoulder Elbow Surg 2021;30:1207-13. https://doi.org/10.1016/j.jse.2020.08.009.
2. Aibinder WR, Bartels DW, Sperling JW, Sanchez-Sotelo J. Mid-term radiological results of a cementless short humeral component in anatomical and reverse shoulder arthroplasty. Bone Joint J 2019;101 B:610-4. https://doi.org/10.1302/0301-620X.101B5.BJJ-2018-1374.R1.
3. Bergmann G, Graichen F, Bender A, Rohlmann A, Halder A, Beier A, et al. In vivo gleno-humeral joint loads during forward flexion and abduction. J Biomech 2011;44:1543-52. https://doi.org/10.1016/j.jbiomech.2011.02.142.
4. Bergmann G, Graichen F, Rohlmann A, Westerhoff P, Heinlein B, Bender A, et al. Design and calibration of load sensing orthopaedic implants. J Biomech Eng 2008;130:021009. https://doi.org/10.1115/1.2898831.
5. Bogle A, Budge M, Richman A, Miller RJ, Wiater JM, Voloshin I. Radiographic results of fully uncemented trabecular metal reverse shoulder system at 1 and 2 years' follow-up. J Shoulder Elbow Surg 2013;22:e20-5. https://doi.org/10.1016/j.jse.2012.08.019.
6. Boileau P, Walch G. The three-dimensional geometry of the proximal humerus. Implications for surgical technique and prosthetic design. J Bone Joint Surg Br 1997;79:857-65.
7. Casagrande DJ, Parks DL, Torngren T, Schrumpf MA, Harmsen SM, Norris TR, et al. Radiographic evaluation of short-stem press-fit total shoulder arthroplasty: short-term follow-up. J Shoulder Elbow Surg 2016;25:1163-9. https://doi.org/10.1016/j.jse.2015.11.067.
8. Crosnier EA, Keogh PS, Miles AW. A novel method to assess primary stability of press-fit acetabular cups. Proc Inst Mech Eng H 2014;228:1126-34. https://doi.org/10.1177/0954411914557714.
9. Denard PJ, Noyes MP, Walker JB, Shishani Y, Gobezie R, Romeo AA, et al. Proximal stress shielding is decreased with a short stem compared with a traditional-length stem in total shoulder arthroplasty. J Shoulder Elbow Surg 2017;27:53-8. https://doi.org/10.1016/j.jse.2017.06.042.
10. Dunham CE, Takaki SE, Johnson JA, Dunning CE. Mechanical properties of cancellous bone of the distal humerus. Clin Biomech 2005;20:834-8. https://doi.org/10.1016/j.clinbiomech.2005.05.014.
11. Favre P, Seebeck J, Thistlethwaite PAE, Obrist M, Steffens JG, Hopkins AR, et al. In vitro initial stability of a stemless humeral implant. Clin Biomech 2016;32:113-7. https://doi.org/10.1016/j.clinbiomech.2015.12.004.
12. Graichen F, Arnold R, Rohlmann A, Bergmann G. Implantable 9-Channel telemetry system for in vivo load measurements with orthopedic implants. IEEE Trans Biomed Eng 2007;54:253-61. https://doi.org/10.1109/TBME.2006.886857.
13. Huiskes R, Weinans H, Grootenboer HJ, Dalstra M, Fudala B, Slooff TJ. Adaptive bone-remodeling theory applied to prosthetic-design analysis. J Biomech 1987;20:1135-50.
14. Huiskes R, Weinans H, van Rietbergen B. The relationship between stress shielding and bone resorption around total hip stems and the effects of flexible materials. Clin Orthop Relat Res 1992;274:124-34.
15. Jost PW, Dines JS, Griffith MH, Angel M, Altchek DW, Dines DM. Total shoulder arthroplasty utilizing Mini-stem humeral components: technique and short-term results. HSS J 2011;7:213-7. https://doi.org/10.1007/s11420-011-9221-4.
16. Kikinis R, Pieper SD, Vosburgh KG. 3D Slicer: a Platform for subject-specific image analysis, visualization, and clinical support. In: Intraoperative imaging and image-guided therapy. New York: Springer; 2014. p. 277-89.
17. Knowles NK, Reeves JM, Ferreira LM. Quantitative Computed Tomography (QCT) derived Bone Mineral Density (BMD) in finite element studies: a review of the literature. J Exp Orthop 2016;3:1-16. https://doi.org/10.1186/s40634-016-0072-2.
18. Langohr GDG, Reeves J, Roche CP, Faber KJ, Johnson JA. The effect of short-stem humeral component sizing on humeral bone stress. J Shoulder Elbow Surg 2020;29:761-7. https://doi.org/10.1016/j.jse.2019.08.018.
19. Lill H, Hepp P, Korner J, Kassi JP, Verheyden AP, Josten C, et al. Proximal humeral fractures: how stiff should an implant be? A comparative mechanical study with new implants in human specimens. Arch Orthop Trauma Surg 2003;123:74-81. https://doi.org/10.1007/s00402-002-0465-9.
20. Lucas RM, Hsu JE, Gee AO, Neradilek MB, Matsen FA. Impaction autografting: bone-preserving, secure fixation of a standard humeral component. J Shoulder Elbow Surg 2016;25:1787-94. https://doi.org/10.1016/j.jse.2016.03.008.
21. Macdonald W, Carlsson LV, Charnlcy GJ, Jacobsson CM. Press-fit acetabular cup fixation: principles and testing. Proc Inst Mech Eng H 1999;213:33-9.
22. Mason R, Buckley T, Southgate R, Nicandri G, Miller R, Voloshin I. Radiographic study of humeral stem in shoulder arthroplasty after lesser tuberosity osteotomy or subscapularis tenotomy. Am J Orthop (Belle Mead NJ) 2018;47:1-15. https://doi.org/10.12788/ajo.2018.0036.
23. McElwain JP, English E. The early results of porous-coated total shoulder arthroplasty. Clin Orthop Relat Res 1987;218:217-24.
24. Melis B, DeFranco M, Lädermann A, Molé D, Favard L, Nérot C, et al. An evaluation of the radiological changes around the grammont reverse geometry shoulder arthroplasty after eight to 12 years. J Bone Joint Surg Br 2011;93 B:1240-6. https://doi.org/10.1302/0301-620X.93B9.25926.
25. Nagels J, Stokdijk M, Rozing PM. Stress shielding and bone resorption in shoulder arthroplasty. J Shoulder Elbow Surg 2003;2746:35-9. https://doi.org/10.1067/mse.2003.22.
26. Pilliar RM, Lee JM, Maniatopoulos C. Observations on the effect of movement on bone ingrowth into porous-surfaced implants. Clin Orthop Relat Res 1986:108-13.
27. Raiss P, Edwards TB, Deutsch A, Shah A, Bruckner T, Loew M, et al. Radiographic changes around humeral components in shoulder arthroplasty. J Bone Joint Surg Am 2014;96:e54(1-9). https://doi.org/10.2106/JBJS.M.00378.
28. Raiss P, Schnetzke M, Wittmann T, Kilian CM, Edwards TB, Denard PJ, et al. Postoperative radiographic findings of an uncemented convertible short stem for anatomic and reverse shoulder arthroplasty. J Shoulder Elbow Surg 2019;28:715-23. https://doi.org/10.1016/j.jse.2018.08.037.
29. Razfar N, Reeves JM, Langohr DG, Willing R, Athwal GS, Johnson JA. Comparison of proximal humeral bone stresses between stemless, short stem, and standard stem length: a finite element analysis. J Shoulder Elbow Surg 2016;25:1076-83. https://doi.org/10.1016/j.jse.2015.11.011.
30. Reeves JM, Athwal GS, Johnson JA. An assessment of proximal humerus density with reference to stemless implants. J Shoulder Elbow Surg 2018;27:641-9. https://doi.org/10.1016/j.jse.2017.09.019.
31. Sanchez-Sotelo J, Wright TW, O'Driscoll SW, Cofield RH, Rowland CM. Radiographic assessment of uncemented humeral components in total shoulder arthroplasty. J Arthroplasty 2001;16:180-7.
32. Schnetzke M, Coda S, Raiss P, Walch G, Loew M. Radiologic bone adaptations on a cementless short-stem shoulder prosthesis. J Shoulder Elbow Surg 2016;25:650-7. https://doi.org/10.1016/j.jse.2015.08.044.
33. Schnetzke M, Loew M, Raiss P, Walch G. Short-stem anatomical shoulder replacement—a systematic review. Obere Extrem 2019;14:139-48. https://doi.org/10.1007/s11678-019-0514-4.
34. Tavakoli A, Spangenberg G, Reeves JM, Faber KJ, Langohr GDG. Humeral short stem varus–valgus alignment affects bone stress. J Orthop Res 2021;40:1-10. https://doi.org/10.1002/jor.25239.
35. Vijayakumar V, Quenneville CE. Quantifying the regional variations in the mechanical properties of cancellous bone of the tibia using indentation testing and quantitative computed tomographic imaging. Proc Inst Mech Eng H 2016;230:588-93. https://doi.org/10.1177/0954411916642800.
36. Westerhoff P, Graichen F, Bender A, Halder A, Beier A, Rohlmann A, et al. In vivo measurement of shoulder joint loads during activities of daily living. J Biomech 2009;42:1840-9. https://doi.org/10.1016/j.jbiomech.2009.05.035.
37. Wolff J. The Law of bone Remodelling. Berlin: Springer; 1986.